Photoinduced electron transfer in $WO_3/BiVO_4$ heterojunction photoanodes: Effects of the WO_3 layer thickness

Ivan Grigioni, Maria Vittoria Dozzi and Elena Selli*

Dipartimento di Chimica, Università degli Studi di Milano, via Golgi 19, I-20133 Milano, Italy

E-mail: elena.selli@unimi.it

Abstract

The photoelectrochemical performance of $WO_3/BiVO_4$ heterojunction photoanodes with a fixed $BiVO_4$ thick top layer and different WO_3 layer thicknesses was investigated under backside irradiation, in comparison with the performance of the same electrodes without top $BiVO_4$ layer. While the performance of these latter increase with increasing WO_3 thickness, the presence of a $BiVO_4$ layer, besides leading to an effective sensitization up to 520 nm, leads to a decrease of incident photon to current efficiency in the short wavelengths range. After having excluded major WO_3 filter effects, this has been attributed to charge carrier recombination effects occurring when both oxides get excited and becoming more relevant with increasing WO_3 thickness and decreasing excitation wavelength.

Keywords: $WO_3/BiVO_4$ heterojunction, photoanode, incident photon to current efficiency, photoproduced charge carriers

1. INTRODUCTION

The photoelectrochemical (PEC) production of renewable solar fuels is a promising way to achieve sustainable solar energy conversion and storage in chemical form [1]. $BiVO_4$, having a 2.4 eV band gap energy and thus being able to absorb ca. 8% of the solar spectrum, appears as a very attractive transition metal semiconductor oxide to be employed as photoanode material for oxygen evolution in PEC cells for water splitting [2–4]. However, the rather low charge carrier mobility within this oxide, together with the slow hole transfer for water oxidation [5–7], severely limits the solar energy to fuel conversion efficiency which can be attained with pure $BiVO_4$.

Much larger charge separation efficiency, and thus a higher overall PEC performance, can be attained if $BiVO_4$ is combined with WO_3 in a heterojunction system [8–12]. Indeed, these two semiconductor oxides have band edge positions that allow the transfer of electrons photoexcited in $BiVO_4$ conduction band (CB) into the lower lying CB of WO_3. Thanks to the higher charge mobility within WO_3, transferred electrons can rapidly diffuse to the external circuit, while photoproduced holes may accumulate in $BiVO_4$. By this way the $WO_3/BiVO_4$ composite heterojunction takes advantage of both the good visible light absorption ability of $BiVO_4$ and the excellent charge transfer properties of WO_3.

We recently investigated the charge carrier dynamics following photon absorption in the $WO_3/BiVO_4$ composite heterojunction photoanodes by means of ultrafast transient absorption (TA) spectroscopy. The first studies, performed upon excitation at 387 nm in Prof. Kamat's laboratory, evidenced a positive TA signal in the visible region [9], which was attributed to holes trapped in $BiVO_4$, in agreement with previous reports [13–15], no signal having been recorded from WO_3 under such conditions. The TA signal was fitted to a bi-exponential decay model for both $BiVO_4$ and $WO_3/BiVO_4$ and the two associated decay lifetimes were ascribed to the depletion

of holes trapped in $BiVO_4$ due to their recombination with CB free electrons and with trapped electrons, respectively. However, by comparing the time constant values obtained with the $WO_3/BiVO_4$ coupled system with those obtained with single $BiVO_4$, we surprisingly found that upon excitation at 387 nm the time component related to the recombination between trapped holes and free electrons in $WO_3/BiVO_4$ (18 ps) was slightly shorter than in pure $BiVO_4$ (24 ps).

The dynamics associated with the electron transfer paths and their rates were fully elucidated by performing femtosecond TA experiments in the visible range, upon excitation at different wavelengths [16]. In fact, when $BiVO_4$ in the heterojunction is selectively excited, e.g. by pumping at 500 nm, the overall recombination between electrons and holes becomes slower than in single $BiVO_4$, because of the injection of photoexcited electrons from the CB of $BiVO_4$ into the CB of WO_3.

The dynamics of photopromoted electrons in these systems was also probed by directly tracking the TA signal of photoexcited electrons in the mid-infrared region, in the picosecond to microsecond timescale [17]. In pure $BiVO_4$ the mid-IR TA signal was found to decay within a few hundreds of picosecond, with a faster dynamics than the holes TA signal tracked in the visible, possibly due to the fast relaxation of free electrons to states unobservable in the mid-IR region [18]. The lifetime increase of trapped electrons in $WO_3/BiVO_4$ upon 500 nm excitation perfectly parallels that obtained for trapped holes by monitoring TA in the visible region. Finally, uncontroversial evidence of electron transfer from the $BiVO_4$ CB to the WO_3 was obtained by mid-IR TA experiments up to the microsecond timescale. In fact, upon selective $BiVO_4$ excitation in the heterojunction a mid-IR long lasting signal was observed, which can be originated exclusively by long-lived electrons in WO_3, as free electrons photopromoted in $BiVO_4$ decay within 1 ns. On the other hand, when both oxides get excited, e.g. by pumping at 387 nm, trapped holes in the

$WO_3/BiVO_4$ coupled system recombine faster than in $BiVO_4$ alone [16], because a new electron-hole recombination channel becomes active, i.e. the recombination between the electrons excited in the WO_3 CB and the holes trapped in $BiVO_4$.

Aiming at optimizing the thickness of the two oxide layers in the heterojunction and also getting a better insight into the effects of this back electron transfer from WO_3 to the $BiVO_4$ valence band (VB), in the present work we investigate the effect that an increasing thickness of the WO_3 layer has on the PEC performance of WO_3 and $WO_3/BiVO_4$ photoanodes upon excitation at 400 nm, i.e. under conditions in which both semiconductors get excited.

2. EXPERIMENTAL SECTION

Photoelectrodes preparation. Single layer WO_3 photoanodes were prepared by spin coating deposition of a WO_3 layer on a fluorine-doped tin oxide (FTO) glass electrode, followed by calcination [9]. In a typical procedure, 1.0 mL of an ethanol solution containing 5 wt% of tungsten ethoxide was added to citric acid (42 mg), acting as stabilizer, under dry conditions to avoid tungsten ethoxide hydrolysis. After complete citric acid dissolution, 0.3 mL of benzyl alcohol and then 40 mg of ethyl cellulose were also added to the solution, which was stirred for 1 h at 70 °C and then at room temperature overnight, to ensure complete ethyl cellulose swelling. The so prepared paste had a 0.085 M tungsten content. The WO_3 layer was obtained by depositing 100 μL of this paste on a 2.5 x 2.5 cm^2 clean FTO glass electrode, followed by spin coating at 6000 rpm for 30 s, drying at 80 °C for 1 h and annealing at 500 °C for 1 h.

The multilayered WO_3 photoanodes were obtained by repeatedly spin coating 100 μL of the precursor paste onto the FTO substrate, followed by drying at 70 °C for 10 min and annealing at 450 °C for 15 min. These three steps (deposition, drying and annealing) constitute a single layer preparation cycle. Photoanodes with increasing WO_3 thickness were obtained by repeating this

cycle 2, 4, and 6 times; they were labelled WO_3 (nL), with n = 2, 4, 6 referring to the number of deposited WO_3 layers. All photoanodes were finally annealed at 500 °C for 1 h.

The $WO_3/BiVO_4$ combined photoanodes were prepared by coating the so obtained multilayered WO_3 electrodes with a $BiVO_4$ film, following a procedure similar to that already reported elsewhere [19]. Starting from 6 mL of a 23.3% HNO_3 solution containing 0.004 mol of citric acid, $Bi(NO_3)_3$ and NH_4VO_3 (0.002 mol) were added first, followed by the addition of 0.04 g of poly(vinyl alcohol) and 0.25 mL of acetic acid, to obtain a denser paste. The mixture was stirred up to complete poly(vinyl alcohol) dissolution. 80 µL of this paste were then spin coated at 4000 rpm for 30 s on a FTO/WO_3 electrode, to obtain a top $BiVO_4$ layer. The $WO_3/BiVO_4$ photoanodes were obtained after drying these multilayered systems for 1 h at 80 °C, followed by annealing for 1 h at 500 °C; they were labelled WO_3 (nL)/$BiVO_4$, with n = 2, 4, 6 (see Scheme 1).

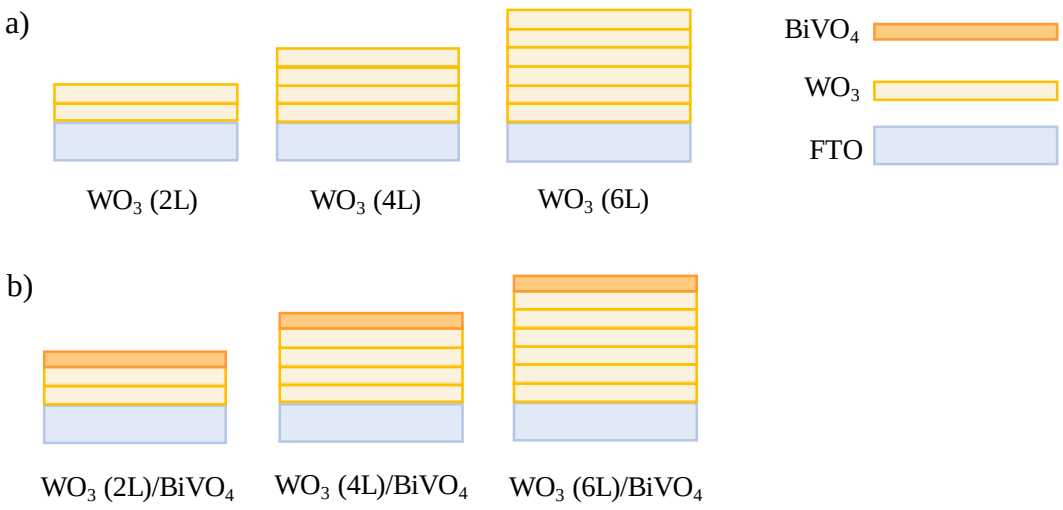

Scheme 1. (a) 2-, 4- and 6-layered WO_3 photoanodes,(b) afterwards covered with a $BiVO_4$ layer. The overall thickness of the WO_3 layers in both WO_3(nL) and WO_3(nL)/$BiVO_4$ photoelectrodes was 75 nm, 150 nm and 210 nm for n = 2, 4 and 6, respectively; the thickness of the top $BiVO_4$ layer in WO_3(nL)/$BiVO_4$ photoelectrodes was 50 nm.

In order to exclude any day to day variation in the deposition conditions, all $WO_3/BiVO_4$ photoanodes of the present investigation were prepared in the same day.

Optical, structural and photoelectrochemical tests. A Jasco V-670 spectrophotometer was employed to record the absorption spectra of the photoelectrodes in the transmittance mode. The crystalline phase of the materials was determined through X-ray powder diffraction (XRPD) analysis using a Philips PW1820 instrument with Cu Kα radiation at 40 mA and 40 kV. The average WO_3 layer thickness was evaluated by means of a Bruker DektakXT profilometer equipped with a 12.5 μm radius stylus, operating at a stylus force of 3 mg. Field-emission scanning electron microscopy (FESEM) images were collected by using a Zeiss SUPRA 40 scanning electron microscope, operating at a 5−7 kV accelerating voltage, with a 3−4 mm working distance.

A three electrode cell, with an Ag/AgCl (3.0 M NaCl) reference electrode, a platinum gauze as a counter electrode and a Princeton Applied Research 2263 (PARstat) potentiostat, was employed in photoelectrochemical (PEC) smeasurements. The photoanodes were tested under back side illumination (i.e. through the $FTO/WO_3/BiVO_4$ interface) in contact with a 0.5 M Na_2SO_4 aqueous solution. Some experiments were also performed in contact with a 0.5 M Na_2SO_3 aqueous solution, acting as hole scavenger, which was buffered at pH 7 with a 0.5 M potassium phosphate buffer [20].

An Oriel, Model 81172 solar simulator providing AM 1.5 G illumination with 100 mW cm^{-2} intensity (1 sun) was employed as irradiation source. All semiconductor oxides are stable at neutral pH and no noticeable degradation was observed under irradiation. The potential vs. Ag/AgCl was converted into the RHE scale using the Nernst equation: $E_{RHE} = E_{AgCl} + 0.059\ pH + E^{o}_{AgCl}$, with E^{o}_{AgCl} (3.0 M NaCl) = 0.210 V at 25 °C. All RHE values refer to pH=0, i.e. they coincide with

SHE values. Linear sweep voltammetry (LSV) scans were recorded at 10 mV s^{-1} starting from the open circuit potential after 5 min irradiation, up to 1.4 V vs. RHE.

Incident photon to current efficiency (IPCE) was measured in a 0.5 M Na_2SO_4 aqueous solution under a 1.23 V applied bias *vs.* RHE, employing the same three electrode cell employed in PEC experiments, with a LOT-Oriel Omni-λ 150 monochromator placed between the Xe lamp and the sample. The current was measured within the 350 to 550 nm range, with a 5 nm step. The incident light power at each wavelength was measured using a Thorlabs PM200 power meter equipped with a calibrated silicon photodiode detector. The following equation was employed to calculate the IPCE at each wavelength λ (nm):

$$\text{IPCE} = \frac{[1240 \times J]}{P_\lambda \times \lambda} \times 100$$

J being the photocurrent density (mA cm^{-2}) and P_λ (mW cm^{-2}) the power of the monochromatic light at λ.

To better highlight the wavelength-dependent PEC performance of the coupled systems, the IPCE values of each WO_3 (nL)/$BiVO_4$ heterojunction electrode were compared with those obtained with the corresponding WO_3 (nL) photoanodes by means of the IPCE enhancement factor calculated as follows:

$$\text{IPCE enhancement} = \text{IPCE}_{\text{WO}_3\text{(nL)/BiVO}_4} - (\text{IPCE}_{\text{WO}_3\text{(nL)}} + \text{IPCE}_{\text{BiVO}_4})$$

where ($\text{IPCE}_{\text{WO}_3\text{(nL)/BiVO}_4}$) is the IPCE measured with the coupled system, while ($\text{IPCE}_{\text{WO}_3\text{(nL)}}$ and $\text{IPCE}_{\text{BiVO}_4}$ are the IPCEs of the WO_3 (nL) and $BiVO_4$ photoanodes recorded in separate experiments.

3. RESULTS AND DISCUSSION

Photoanodes characterization. The X-ray powder diffraction (XRPD) patterns of the investigated photoanodes confirmed the presence of monoclinic structures (JCPDS 05-0363 for WO_3 and JCPDS 75-1867 for $BiVO_4$), in both individual and combined electrodes. The film thickness, evaluated through profilometry, increased by slightly less than 40 nm for each WO_3 deposition cycle, the thickness of WO_3 (2L), WO_3 (4L) and WO_3 (6L) being 75 nm, 150 nm and 210 nm, respectively. In all coupled systems the $BiVO_4$ layer was 50 nm thick.

The successful deposition of $BiVO_4$ on the differently thick WO_3 films was confirmed by the FESEM top views of $WO_3/BiVO_4$ electrodes, such as that reported in figure 1(a). In fact, a network of aggregated particles is evidenced, with morphological features similar to those obtained for pure $BiVO_4$ films prepared by the same procedure, which are significantly different with respect to those appearing in the top view of pure WO_3 films (see fig. 1(b)).

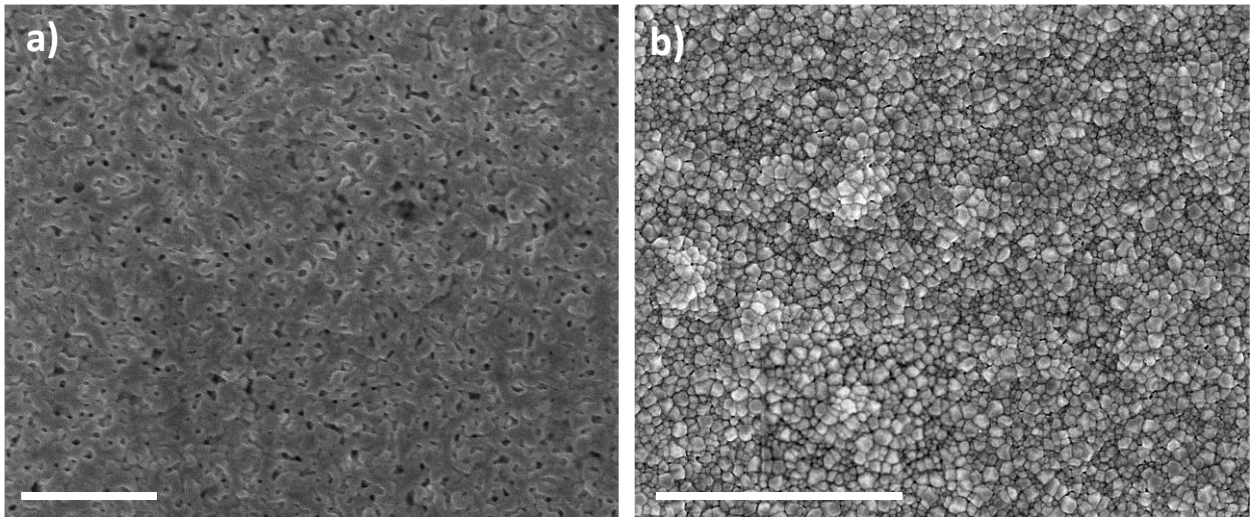

Figure 1. FESEM top view images of (a) $WO_3/BiVO_4$ and (b) WO_3 photoanodes. The scale bar is 1 μm.

Figure 2 shows the absorption spectra of the here investigated WO_3 (nL) and WO_3 (nL)/$BiVO_4$ photoelectrodes, together with that of a 50 nm thick $BiVO_4$ photoanode. All WO_3 multilayered films show a good transparency in the visible region, in line with the WO_3 band gap of ca. 2.7 eV, while the absorbance below 450 nm (the WO_3 absorption onset) increases with the number of WO_3 layers. A similar absorbance increase trend below 400 nm with increasing WO_3 thickness is also preserved in WO_3/$BiVO_4$ coupled films, all of which exhibit an absorption onset red-shifted to around 520 nm due to the presence of the $BiVO_4$ layer and a similar absorption around 420 nm, almost independent of the number of WO_3 layers. Residual absorption above 550 nm is due to light scattering.

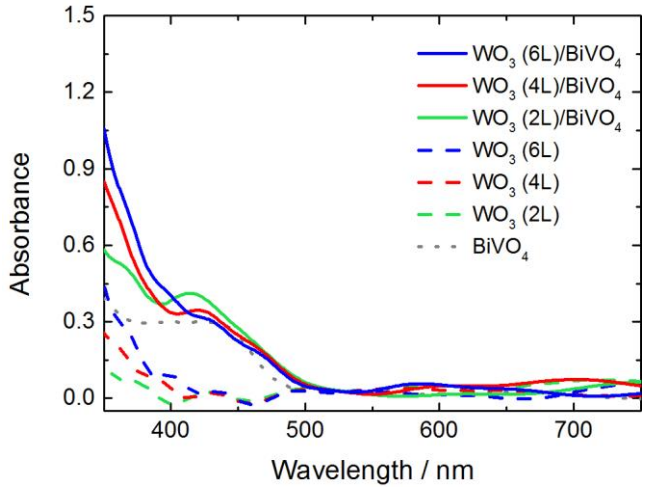

Figure 2. Absorption spectra of the WO_3 multilayer films, of the corresponding WO_3/$BiVO_4$ coupled electrodes and of individual 50 nm thick $BiVO_4$.

Photoelectrochemical properties of multilayers WO_3 – based electrodes. The linear sweep voltammetry (LSV) curves recorded with individual WO_3 or with the corresponding coupled WO_3/$BiVO_4$ photoanodes with different WO_3 thickness can be compared in figure 3, in terms of photocurrent density vs. applied potential (*J*–*V*) plots under AM 1.5 G, 100 mW cm^{-2} illumination,

in contact with a 0.5 M Na_2SO_4 aqueous solution. Individual $BiVO_4$ shows a low photocurrent response.

In the case of WO_3 (nL) series electrodes, a progressive increase in photocurrent is observed with increasing number of WO_3 layers, as a consequence of their relatively higher absorption properties. A significantly higher photocurrent is attained upon deposition of the $BiVO_4$ layer on the multilayer WO_3 electrodes, arising from the improved charge separation at the heterojunction, as already demonstrated for the coupled material containing a single WO_3 layer [9]. Indeed, both the conduction and valence band edges of $BiVO_4$ are more negative in energy than those of WO_3, leading to a type II band alignment. This facilitates photoproduced charge separation, photopromoted electrons tending to accumulate in WO_3 and photogenerated holes tending to accumulate in $BiVO_4$, with the consequent decrease of the electron-hole recombination rate, which is quite high in pure $BiVO_4$.

However, as shown in figure 3, while the current density increases with increasing WO_3 layer thickness in WO_3 (nL) electrodes, in WO_3 (nL)/$BiVO_4$ electrodes the photocurrent density slightly decreases with increasing the WO_3 layer thickness, on the whole range of applied bias.

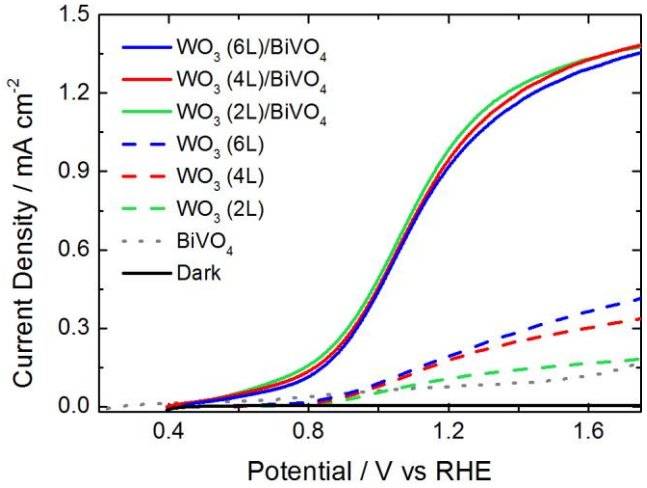

Figure 3. Linear sweep voltammetry under AM 1.5 G irradiation of the WO_3 (nL) and WO_3 (nL)/$BiVO_4$ photoanodes, recorded in 0.5 M Na_2SO_4 aqueous solutions**.**

A better insight into this unexpected trend was obtained through wavelength-dependent PEC measurements, performed at a fixed bias of 1.23 V vs. RHE. The incident photon to current efficiency (IPCE) responses of all photoanodes in 0.5 M Na_2SO_4 solutions are shown in figure 4(A).

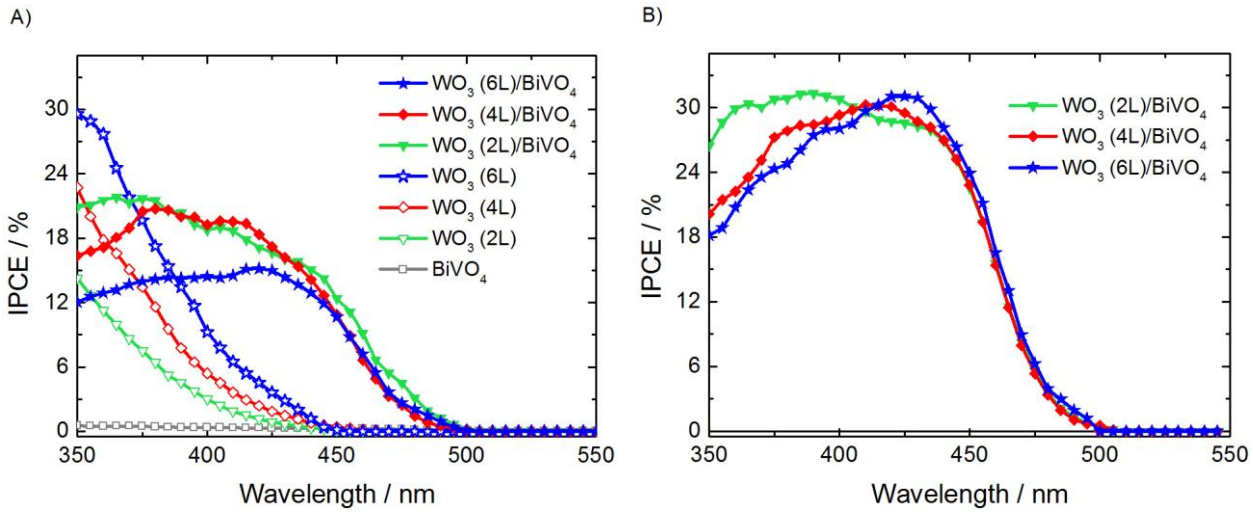

Figure 4. IPCE recorded at 1.23 V vs. RHE (A) in 0.5 M Na_2SO_4 solutions with the WO_3 multilayer electrodes (empty symbols), with the corresponding $WO_3/BiVO_4$ coupled photoanodes (full symbols) and with an individual $BiVO_4$ electrode; (B) with the $WO_3/BiVO_4$ coupled electrodes in 0.5 M Na_2SO_3 solutions buffered at pH 7.

This figure first of all demonstrates that the enhanced photocurrent generated in WO_3 (nL) materials with increasing the WO_3 layer thickness (see figure 3) is due to the systematic IPCE improvement in the whole range of WO_3 absorption, i.e. up to 450 nm, when passing from WO_3 (2L) to WO_3 (6L). Furthermore, figure 4(A) also shows that the presence of the $BiVO_4$ top layer determines an effective visible light sensitization of the WO_3-based photoanodes, all combined WO_3 (nL)/$BiVO_4$ electrodes exhibiting a photocurrent onset red-shifted to ca. 510 nm, while $BiVO_4$ alone shows an almost negligible IPCE. However, this sensitization effect at short wavelengths decreases with increasing the WO_3 layer thickness, so that at wavelengths shorter

than 390 nm the IPCE values obtained with the WO_3 (6L)/$BiVO_4$ electrode are even lower than those attained with the WO_3 (6L) electrode.

Similar IPCE trends, though with higher IPCE values, were obtained in PEC tests performed with the WO_3 (nL)/$BiVO_4$ coupled electrodes in contact with an electron donor containing solution, i.e. a 0.5 M Na_2SO_3 aqueous solution, as shown in figure 4(B). Hole scavenger species, such as Na_2SO_3, are employed to suppress charge recombination processes at the electrode/electrolyte interface, affecting the slow water oxidation reaction. The similar behavior observed in contact with the two electrolyte solutions with increasing the number of WO_3 layers in the coupled WO_3/$BiVO_4$ photoanodes excludes that the origin of the IPCE decrease below 390 nm observed with WO_3 (nL)/$BiVO_4$ coupled electrodes is due to surface recombination processes and indicates that it should rather be ascribed to bulk electronic effects in the coupled materials.

This wavelength dependent behavior of the photocurrent values of the WO_3/$BiVO_4$ photoanodes can be better appreciated by considering their IPCE enhancement factor, defined in Section 2 and calculated from the IPCE values determined in contact with the Na_2SO_4 solutions, which is reported in figure 5.

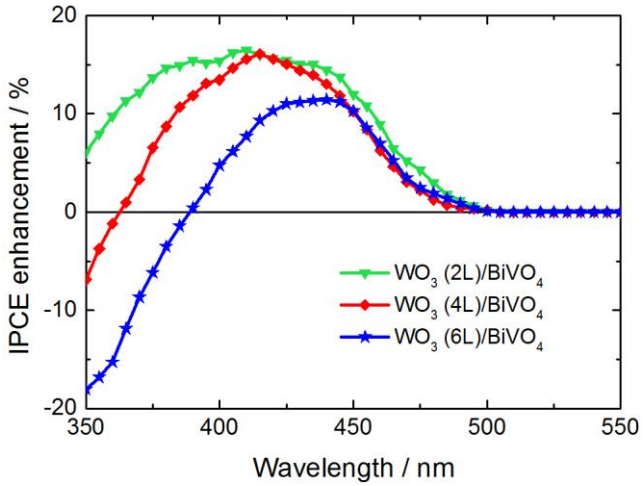

Figure 5. IPCE enhancement factor calculated from the IPCE data for the WO_3/$BiVO_4$ coupled electrodes.

The IPCE enhancement factor is clearly almost unaffected by the WO_3 layer width under irradiation at wavelengths longer than ca. 450 nm, i.e. with an associated energy lower than the WO_3 band gap. Indeed, under such conditions selective $BiVO_4$ excitation occurs, followed by beneficial charge carrier separation at the $WO_3/BiVO_4$ heterojunction, due to the flow of the electron photopromoted in the CB of $BiVO_4$ into the CB of WO_3 (Scheme 2(a)). This leads to enhanced PEC performances independent of the WO_3 thickness.

However, upon excitation at wavelengths lower than ca. 450 nm, the IPCE enhancement factor obtained with coupled photoanodes with different WO_3 layer thickness exhibits a different trend, depending on the thickness of the WO_3 layer. In particular, for the thickest WO_3 layer (i.e. for the WO_3 (6L)/$BiVO_4$ electrode) the IPCE enhancement factor starts to decrease below 450 nm. The same occurs for the WO_3 (4L)/$BiVO_4$ and WO_3 (2L)/$BiVO_4$ coupled electrodes, with their enhancement factor decline starting at progressively shorter wavelength with decreasing number of WO_3 layers (see figure 5).

As irradiation was performed under back side configuration, i.e. through the FTO/WO_3/$BiVO_4$ interface, we estimated the possible filter effect of the WO_3 layer at wavelengths shorter than 450 nm, which would decrease the amount of light reaching the sensitizing $BiVO_4$ layer. Therefore, on the basis of the absorption spectra shown in figure 2, the percent amount of incident photons absorbed by WO_3 or $BiVO_4$ in the coupled systems was evaluated, as a function of both the incident wavelength and the number of WO_3 layers. In particular, absorption ascribed to WO_3 was directly calculated from the corresponding absorption spectra of the WO_3 (nL) series electrodes, while the percent amount of photons absorbed by the $BiVO_4$ layer in each combined electrode was calculated

as the difference between the absorption of WO_3 (nL)/$BiVO_4$ films and that of the corresponding WO_3 (nL) film. The results are reported in Table 1, together with the absorption of pure $BiVO_4$.

Table 1. Percent amounts of incident photons absorbed by WO_3 and $BiVO_4$ in WO_3 (nL)/$BiVO_4$, at different wavelengths and for different numbers of WO_3 layers (nL, n = 2, 4, 6). The percent amount of photons absorbed by individual $BiVO_4$ is also reported for comparison.

	WO_3 (nL)/$BiVO_4$ coupled system						**pure $BiVO_4$**
	Photons Absorbed by WO_3 (%)			Photons Absorbed by $BiVO_4$ (%)			Absorbed photons (%)
λ (nm)	2L	4L	6L	2L	4L	6L	
350	27	45	65	46	41	26	60
360	18	39	52	53	42	34	55
370	15	28	45	50	45	36	51
380	12	20	28	50	45	43	49
390	9	17	21	49	42	44	50
400	7	9	19	52	44	41	50
410	4	5	12	53	49	43	50
420	3	3	9	54	52	43	50
430	2	2	5	52	52	45	50
440	1	2	3	50	46	41	49
450	0	0	0	46	44	40	44

In the 390-450 nm wavelength range, the percent amount of photons absorbed by the $BiVO_4$ layer in WO_3/$BiVO_4$ heterojunction electrodes was found to become only slightly lower with increasing WO_3 layer thickness, possibly due to scattering effects, without any very significant variation (ca. ± 10% maximum) with respect to the light absorbed in the pure $BiVO_4$ electrode. Thus, the systematic drop of the IPCE enhancement factor observed in the 450 to 390 nm

wavelength range with increasing the WO_3 thickness (figure 5) cannot be ascribed exclusively to the different $BiVO_4$ absorption ability in the coupled systems.

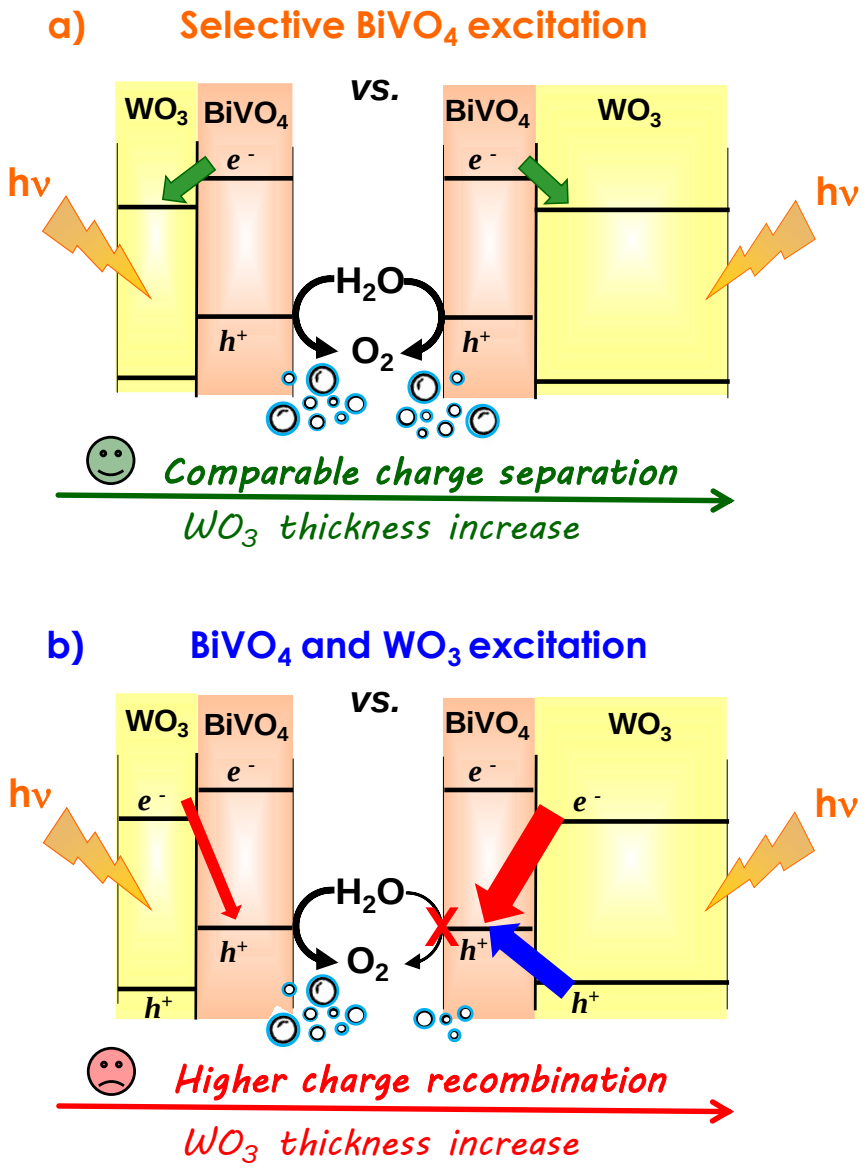

Scheme 2. Wavelength dependent charge carrier interaction occurring in the $WO_3/BiVO_4$ coupled electrodes under (a) selective $BiVO_4$ excitation (λ_{exc} > 450 nm) or (b) simultaneous $BiVO_4$ and WO_3 excitation (λ_{exc} < 450 nm).

Furthermore, the IPCE enhancement factors of the investigated coupled systems reported in figure 5 clearly evidence that the overall efficiency of WO_3 (4L)/$BiVO_4$ and WO_3 (6L)/$BiVO_4$ becomes significantly lower than those of the corresponding pure WO_3 electrodes (negative IPCE enhancement factors) at wavelengths shorter than 360 and 390 nm, respectively. After having excluded relevant filter effects, this should be related to detrimental charge carrier recombination occurring under the simultaneous excitation of both semiconductors [16]. Under such conditions, in fact, a recombination channel between photoexcited electrons in WO_3 CB and photogenerated holes in $BiVO_4$ VB may open (red arrows in Scheme 2(b)), which reasonably becomes more relevant as the amount of photopromoted electrons in WO_3 increases due to higher light absorption properties of thicker WO_3 films. Furthermore, upon WO_3 excitation the holes h^+ photoproduced in WO_3 VB may also be transferred into the $BiVO_4$ VB (blue arrow in Scheme 2(b)), which is located at a less positive potential, with a consequent decrease of their oxidative ability and their possible recombination with electrons photopromoted in both WO_3 and $BiVO_4$ CBs. This in turn may also be at the origin of the lower efficiency observed for the two thicker heterojunction photoanodes with respect to the corresponding individual WO_3 ones.

CONCLUSIONS

The PEC performances of WO_3 electrodes may be differently affected by the deposition of a relatively thin layer of $BiVO_4$ (ca. 50 nm) acting as an efficient visible light sensitizer, depending on both the WO_3 film thickness and the irradiation wavelengths region. In fact, a synergy between the two oxides is attained under irradiation at wavelengths longer than the WO_3 absorption edge (450 nm), independently of the WO_3 film thickness, with all coupled systems working significantly better than the two separate materials. On the other hand, upon simultaneous excitation of both semiconductors, the performances of the coupled systems start to decrease in a different way

mainly depending on the WO_3 layer thickness. In this case, undesired charge carrier recombination becomes clearly more marked with increasing the WO_3 layer thickness, WO_3 (4L)/$BiVO_4$ and WO_3 (6L)/$BiVO_4$ behaving even less efficiently than the corresponding pure WO_3 electrodes under irradiation at wavelengths shorter than 360 and 400 nm, respectively.

Acknowledgements

The authors gratefully acknowledge financial support from Fondazione Cariplo 2013-0615 and MIUR PRIN 2015K7FZLH projects. The use of instrumentation purchased through the SmartMatLab project, Fondazione Cariplo grant 2013-1766, is also gratefully acknowledged.

References

[1] Armstrong R C, Wolfram C, de Jong K P, Gross R, Lewis N S, Boardman B, Ragauskas A J, Ehrhardt-Martinez K, Crabtree G and Ramana M V 2016 *Nat. Energy* **1** 15020

[2] Park Y, McDonald K J and Choi K-S 2013 *Chem. Soc. Rev.* **42** 2321–37

[3] Kim T W and Choi K-S 2014 *Science* **343** 990

[4] Kim J H, Jang J-W, Jo Y H, Abdi F F, Lee Y H, Van De Krol R and Lee J S 2016 *Nat. Commun.* **7** 13380

[5] Zhong D K, Choi S and Gamelin D R 2011 *J. Am. Chem. Soc.* **133** 18370–7

[6] Abdi F F, Savenije T J, May M M, Dam B and Van De Krol R 2013 *J. Phys. Chem. Lett.* **4** 2752–7

[7] Zachäus C, Abdi F F, Peter L M and Van De Krol R 2017 *Chem. Sci.* **8** 3712–9

[8] Hong S J, Lee S, Jang J S and Lee J S 2011 *Energy Environ. Sci.* **4** 1781–7

[9] Grigioni I, Stamplecoskie K G, Selli E and Kamat P V. 2015 *J. Phys. Chem. C* **119** 20792–800

[10] Shi X, Herraiz-Cardona I, Bertoluzzi L, Lopez-Varo P, Bisquert J, Park J H and Gimenez S 2016 *Phys. Chem. Chem. Phys.* **18** 9255–61

[11] Chae S Y, Lee C S, Jung H, Joo O S, Min B K, Kim J H and Hwang Y J 2017 *ACS Appl. Mater. Interfaces* **9** 19780–90

[12] Van C N, Do T H, Chen J W, Tzeng W Y, Tsai K A, Song H, Liu H J, Lin Y C, Chen Y C, Wu C L, Luo C W, Chou W C, Huang R, Hsu Y J and Chu Y H 2017 *NPG Asia Mater.* **9** e357

[13] Ma Y, Pendlebury S R, Reynal A, Le Formal F and Durrant J R 2014 *Chem. Sci.* **5** 2964–73

[14] Aiga N, Jia Q, Watanabe K, Kudo A, Sugimoto T and Matsumoto Y 2013 *J. Phys. Chem. C* **117** 9881–6

[15] Ravensbergen J, Abdi F F, Van Santen J H, Frese R N, Dam B, Van De Krol R and Kennis J T M 2014 *J. Phys. Chem. C* **118** 27793–800

[16] Grigioni I, Stamplecoskie K G, Jara D H, Dozzi M V, Oriana A, Cerullo G, Kamat P V. and Selli E 2017 *ACS Energy Lett.* **2** 1362–7

[17] Grigioni I, Abdellah M, Corti A, Dozzi M V, Hammarström L and Selli E 2018 *J. Am. Chem. Soc.* **140** 14042–5

[18] Suzuki Y, Murthy D H K, Matsuzaki H, Furube A, Wang Q, Hisatomi T, Domen K and Seki K 2017 *J. Phys. Chem. C* **121** 19044–52

[19] Su J, Guo L, Yoriya S and Grimes C A 2010 *Cryst. Growth Des.* **10** 856–61

[20] Grigioni I, Corti A, Dozzi M V and Selli E 2018 *J. Phys. Chem. C* **122** 13969–78